

The Effect of Satellite Galaxies on Gravitational Lensing Flux Ratios

E.M. Shin^{*} and N.W. Evans^{*}

Institute of Astronomy, University of Cambridge, Madingley Road, Cambridge, CB3 0HA, United Kingdom

9 February 2022

ABSTRACT

Gravitational lenses with anomalous flux ratios are often cited as possible evidence for dark matter satellites predicted by simulations of hierarchical merging in cold dark matter cosmologies. We show that the fraction of quads with anomalous flux ratios depends primarily on the total mass and spatial extent of the satellites, and the characteristic lengthscale $d_{1/2}$ of their distribution. If $d_{1/2} \sim 100$ kpc, then for a moderately elliptical galaxy with a line-of-sight velocity dispersion of $\sim 250 \text{ km s}^{-1}$, a mass of $\sim 3 \times 10^9 M_\odot$ in highly-concentrated (Plummer model) satellites is needed for 20% of quadruplets to show anomalous flux ratios, rising to $\sim 1.25 \times 10^{10} M_\odot$ for 50%. Several times these masses are required if the satellites have more extended Hernquist profiles. Compared to a typical elliptical, the flux ratios of quads formed by typical edge-on disc galaxies with maximum discs are significantly less susceptible to changes through substructure – three times the mass in satellite galaxies is needed to affect 50% of the systems.

In many of the lens systems with anomalous flux ratios, there is evidence for visible satellites (e.g., B2045+265 or MG0414+0534). We show that if the anomaly is produced by substructure with properties similar to the simulations, then optically identified substructure should not be preponderant among lens systems with anomalies. There seem to be two possible resolutions of this difficulty. First, in some cases, visible substructure may be projected within or close to the Einstein radius and wrongly ascribed as the culprit, whereas dark matter substructure is causing the flux anomaly. Second, bright satellites, in which baryon cooling and condensation has taken place, may have higher central densities than dark satellites, rendering them more efficient at causing flux anomalies.

Key words: gravitational lensing – dark matter

1 INTRODUCTION

The abundance of substructure in galaxy halos is emerging as a key test in theories of galaxy assembly. In Cold Dark Matter cosmologies, dark matter overdensities collapse to form cusped halos, with the smallest and least massive halos being the densest. The simulations of Klypin et al. (1999) and Moore et al. (1999) predicted hundreds of small Galactic satellite halos, in contrast to the nine then known satellites around the Milky Way. Efstathiou (1992) had already suggested that photoionisation may lengthen the cooling times of gas in haloes with low circular speeds. This effect suppresses the formation of satellite galaxies, but produces a large population of entirely dark satellites (see e.g. Kravtsov et al. 2004; Moore et al. 2006).

In strong lensing, it has been known for some years that simple, smooth models of galaxy lenses usually fitted the image positions well, but the flux ratios of the images poorly. In a bold paper, Dalal & Kochanek (2002) argued that the flux anomalies in gravitational lens systems could be interpreted as evidence for entirely

dark substructures. They used 7 of the then available four-image lens systems to claim detection of substructure amounting to a total mass of 0.6% – 6% of the lens galaxy mass. However, this interpretation was challenged as flux anomalies could arise from alternative sources, such as absorption, scattering, or scintillation by the interstellar medium of the lens galaxy, or by higher order harmonics in the ellipsoidal models used to fit lens systems, or stellar microlensing (see e.g. Evans & Witt 2003; Kochanek & Dalal 2004; Mao et al. 2004). In particular, the surface mass density in substructure as judged from simulations seems to be lower than that required by gravitational lensing, at least within the Einstein radius which probes primarily the inner parts of halos (e.g., Mao et al. 2004). It is also hard to reproduce the observed statistics on cusp violations with substructure (Macciò & Miranda 2006). This argues against substructure as a primary cause of anomalous flux ratios.

Nonetheless, there is good evidence in favour of substructure, and, in some cases, visible substructure can be identified. One of the gravitational lens systems with a flux ratio anomaly is the radio-loud quadruple CLASS B2045+265 discovered by Fassnacht et al. (1999). Recent deep *Hubble Space Telescope* and *Keck* imaging of this system by McKean et al. (2007) have revealed the presence of

^{*} E-mail: ems@ast.cam.ac.uk; nwe@ast.cam.ac.uk

a tidally disrupted dwarf galaxy G2. This may be the cause of the flux ratio anomaly, although caution is needed as modelling suggests that G2 must be very highly flattened ($q = 0.13$). There is also evidence for visible structure – possibly a small galaxy – in the radio-loud quadruple MG0414+0534. Schechter & Moore (1993) already argued that the perturbation caused by this object may account for the relatively poor agreement between the observed data on this lens and the theoretical models. The quadruple lens systems CLASS B1608+656 (see e.g., Fassnacht et al. 1996) has a loose group of galaxies at the same redshift as the main lensing galaxy, a phenomenon that also occurs in the six-image radio-loud system B1359+154 (Rusin et al. 2001). It seems that visible substructure may well be responsible for some of the flux ratio anomalies.

In addition, there have been striking observational developments nearer to home. The last two years have seen the discovery of 10 faint, new Milky Way satellites in data from the Sloan Digital Sky Survey (SDSS, see Willman et al. 2005, Zucker et al. 2006a,b; Belokurov et al. 2006, 2007). It seems likely that a population of ultra-faint, dwarf galaxies does surround the Milky Way. These may be representatives of the “missing satellites”, as predicted by the simulations of Klypin et al. (1999) and Moore et al. (1999), or they may be a population of tidal dwarf galaxies or even star clusters (see e.g., Belokurov et al. 2007). Such ultra-faint objects are only detectable nearby, and so would be – to all intents and purposes – dark at the typical redshifts of strong lenses.

All this suggests that it is worth re-examining the effects of substructure on strong lenses. In this paper, we answer the following questions. Given what we know about the satellite populations, how frequently might we expect anomalous flux ratios for elliptical and spiral galaxies? If luminous satellite galaxies represent the bright and massive end of a predominantly faint population of objects, how frequently might we expect to attribute flux ratio anomalies to visible objects? Three (B2045+265, MG0414+0534, B1608+656) out of the sample of six quadruplets originally identified by Dalal & Kochanek (2002) as anomalous have optically identified companions that are possible causes. At the outset, this seems surprisingly high, if the substructure is predominantly dark.

The paper is arranged as follows. In §2, models of elliptical and spiral galaxies are briefly introduced, together with their satellite galaxy populations. In §3, the frequency with which anomalous flux ratios occur is shown to depend primarily on the scalelength of the satellite distribution, the mass model used for the satellites and the total mass in substructure, while depending only weakly on how the mass is distributed between satellites. The simulations reported in §4 give the expected fraction of anomalous flux ratios for both ellipticals and spiral lenses, together with the typical numbers caused by high mass and luminous satellite galaxies.

2 METHODOLOGY

2.1 Mass Models

For convenience, we follow Schneider et al. (1992) by defining in the lens plane the dimensionless distance, dimensionless surface mass density and critical surface mass density

$$\mathbf{R} = \frac{\hat{\mathbf{R}}}{\xi_0}, \quad \kappa(\mathbf{R}) = \frac{\Sigma(\xi_0 \mathbf{R})}{\Sigma_{\text{cr}}}, \quad \Sigma_{\text{cr}} = \frac{c^2 D_s}{4\pi G D_l D_{ls}}, \quad (1)$$

with D_s , D_l , D_{ls} being the distances to the source, lens, and between lens and source, and ξ_0 an arbitrary scale length which relates the scaled (uncapped) coordinates to the unscaled (capped).

The corresponding dimensionless deflection potential is the solution of the Poisson Equation

$$\kappa(x, y) = \frac{1}{2} \nabla^2 \psi \quad (2)$$

and the dimensionless bending angle is $\alpha = \nabla \psi$.

2.1.1 Primary Lens

We examine two models for the main lens galaxy. The first is appropriate for an elliptical galaxy lens. It is a pseudo-isothermal elliptic deflection potential (see e.g. Kassiola & Kovner 1993; Hunter & Evans 2001; Evans & Hunter 2002)

$$\psi(x, y) = E_r (r_c^2 + (1 - \epsilon)x^2 + (1 + \epsilon)y^2)^{1/2} \quad (3)$$

where r_c is a dimensionless core radius (the length scale being the arbitrarily chosen ξ_0), and

$$E_r = \sigma^2 (\xi_0 G \Sigma_{\text{cr}})^{-1} \quad (4)$$

is the dimensionless Einstein-ring radius of the singular isothermal sphere with line-of-sight velocity dispersion σ corresponding to the $r_c = 0$, $\epsilon = 0$ case. There are two critical curves: a small inner one which maps to a ‘radial’ caustic and an outer ‘tangential’ one which maps to an astroid caustic. At the ranges of ϵ we consider, the astroid caustic is wholly within the outer caustic. A point source has one image if it is outside both caustics, three if it is inside the outer caustic, and five if it is inside the astroid caustic. Triplets and quintuplets, however, are effectively doublets and quadruplets, because one of the multiple images is a highly demagnified central image within the small inner critical curve. For concreteness, we consider the elliptical potential to have (unless otherwise specified) a velocity dispersion $\sigma = 250 \text{ km s}^{-1}$ and a core radius of 100 pc, as suggested by Kassiola & Kovner (1993) and Evans & Hunter (2002). We restrict the ellipticity parameter to be smaller than $\epsilon \approx 0.2$, otherwise the corresponding surface mass density becomes dumbbell-shaped, which is inappropriate for elliptical galaxies (see Kassiola & Kovner 1993).

The second model is appropriate for a spiral galaxy lens. It is a three-component model widely used in galactic astronomy (see e.g. Dinescu et al. 1999, Fellhauer et al. 2006) as a model for the Milky Way. It has a Hernquist (1990) bulge, a Miyamoto-Nagai (1975) disc and a cored isothermal halo. The Hernquist bulge has 3D mass distribution

$$\rho(\hat{r}) = \frac{M_b}{2\pi} \frac{r_b}{\hat{r}(\hat{r} + r_b)^3}, \quad (5)$$

where \hat{r} is the spherical polar radius and r_b a core radius. That of the halo is

$$\rho(\hat{r}) = \frac{\rho_c}{1 + \hat{r}^2/r_h^2}. \quad (6)$$

where r_h is the core radius and ρ_c the central density. The mass distribution of the Miyamoto-Nagai disc is complicated, but the deflection potential in the edge-on case is simple:

$$\psi_d = \frac{1}{2} m_d \log \left[x^2 + (a + \sqrt{b^2 + y^2})^2 \right], \quad (7)$$

where $m_d = M_d / (\pi \Sigma_{\text{cr}} \xi_0^2)$ is the dimensionless mass and a and b control the shape of the distribution. We normalize our disc galaxy lens to the Milky Way, according to the parameters given in Shin & Evans (2007). Disc galaxies give rise to three main different classes of multiple-image configurations (see e.g. Möller & Blain 1998): ‘core triplets’ (in effect, doublets), ‘disc triplets’ (where images

straddle the plane of the disc) and quintuplets (in effect, quadruplets). The small 7-imaging butterfly cusp in the caustic of this edge-on Milky Way is ignored here (see e.g. Shin & Evans 2007).

We choose the redshift of the lens to be 0.46 and that of the source to be 2.15. These are the median redshifts of known 4-image lens systems (see the CASTLES website), omitting those known to have more than one main lens and those without known lens and source redshifts. We use a flat Λ CDM cosmology with $\Omega_m = 0.27$, $\Omega_\Lambda = 0.73$, $H_0 = 71 \text{ km s}^{-1} \text{ Mpc}^{-1}$.

2.1.2 Plummer Model Satellites

The Plummer model is often fitted to observed dwarf spheroidal galaxies (see e.g. McConnachie & Irwin 2006, Wilkinson et al 2002). We give our satellites densities

$$\kappa(r_k) = \kappa_0^{(k)} (1 + \lambda_k^2 r_k^2)^{-2} \quad (8)$$

where $r_k = \sqrt{x_k^2 + y_k^2}$, x_k and y_k being Cartesian coordinates with their origin at the centre of the k th satellite galaxy, $\kappa_0^{(k)}$ is the central density of that galaxy, and $\lambda_k = \xi_0/r_p^{(k)}$ where $r_p^{(k)}$ is the Plummer model scale radius. The mass of any satellite is

$$M_p^{(k)} = \Sigma_{\text{cr}} \kappa_0^{(k)} \pi r_p^{(k)2}. \quad (9)$$

We give a ‘typical’ $10^7 M_\odot$ Plummer satellite a scale radius (equal to its half-light radius) of 140 pc, which is the median half-light radius of known Milky Way satellite spheroidal galaxies (see e.g. Belokurov et al. 2007), and vary r_p as $\sqrt{M_p}$. This mass-radius scaling is consistent with those found in N -body simulations, where the size of satellites scales as a power of the mass. We also put a lower limit on r_p of 70 pc, the smallest known half-light radius of a Milky-Way dwarf spheroidal (Belokurov et al. 2007).

2.1.3 Hernquist Model Satellites

We also examine a second density profile for the satellites, motivated by numerical simulations. The NFW density profile (Navarro et al. 1996)

$$\rho_{\text{NFW}} = \rho_s \left(\frac{\hat{r}}{r_s} \right)^{-1} \left(1 + \frac{\hat{r}}{r_s} \right)^{-2}, \quad (10)$$

is found to be a good fit to cold dark matter subhalos. Rather than using the NFW, which falls off as \hat{r}^{-3} at large radii and therefore has formally infinite total mass, we use the Hernquist density profile, which is similar to the NFW profile, but has an \hat{r}^{-4} asymptotic density decay. Our Hernquist satellites are less concentrated than the Plummers, and we make a lowest order estimate of the effects of tidal stripping by truncating them at tidal radii $\hat{r}_t^{(k)}$ defined by the condition

$$\bar{\rho}^{(k)}(\hat{r}_t^{(k)}) = \bar{\rho}(\hat{r}) \quad (11)$$

where \hat{r} is the radial distance of the k th satellite from the centre of the main galaxy, $\bar{\rho}^{(k)}(\hat{r}_t^{(k)})$ its mean mass density, and $\bar{\rho}(\hat{r})$ the mean mass density due to the main galaxy enclosed within a sphere of radius \hat{r} when the pseudo-isothermal elliptical potential is approximated by a singular isothermal sphere, that is,

$$\bar{\rho}(\hat{r}) = \left(\frac{4}{3} \pi \hat{r}^3 \right)^{-1} \int_0^{\hat{r}} 4\pi \hat{r}'^2 \frac{\sigma^2}{2\pi G \hat{r}'^2} d\hat{r}' = \frac{3\sigma^2}{2\pi G} \hat{r}^{-2}. \quad (12)$$

The truncated Hernquist profile is then

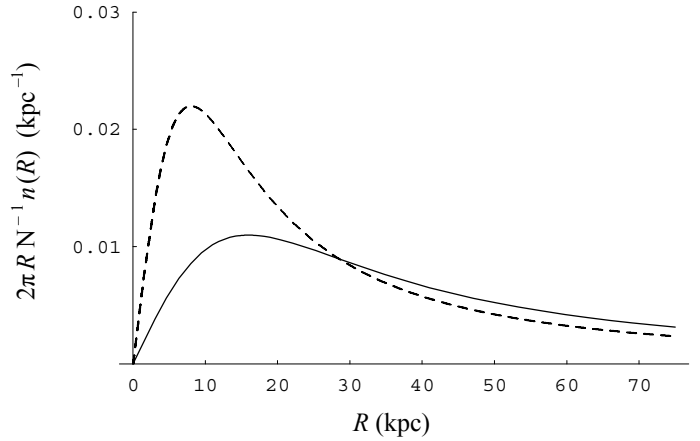


Figure 1. Probability density of satellites with respect to the lens-plane polar radius R . The solid line is for $d_{1/2} = 100$ kpc, the dashed line for $d_{1/2} = 50$ kpc.

$$\rho(\hat{r}_k) = \begin{cases} \frac{M^{(k)}}{2\pi r_s^{(k)2} \hat{r}_k} (1 + \hat{r}_k/r_s^{(k)})^{-3}, & \hat{r} < \hat{r}_t^{(k)} \\ 0, & \hat{r} > \hat{r}_t^{(k)} \end{cases}, \quad (13)$$

where \hat{r}_k is the radial distance from the centre of the k th satellite, $M^{(k)}$ are the untruncated Hernquist masses and $r_s^{(k)}$ are Hernquist scale lengths.

The scale length of each satellite is chosen so that the location of the peak circular velocity of the model (which is r_s) varies with the mass bound within the tidal radius $M_t \equiv M r_t^2 / (r_t^2 + r_s^2)$ as

$$r_s = 10^{-4} \sqrt{M_t/M_\odot} \text{ kpc} \quad (14)$$

in agreement with the numerical simulations of, for example, Diemand, Kuhlen & Madau (2007).

If the tidal radius of any Hernquist satellite is less than its scale radius, we reject it as being too strongly tidally disrupted to be approximated by this mass profile. For example, Metcalf & Madau (2001) find that NFW clumps lose their mass rapidly for $r_t < r_s$. It is beyond the scope of this paper to consider lensing effects due to the tidally-stripped matter from dwarf galaxies.

2.1.4 Spatial Distribution of Satellites

The distribution of satellite galaxies is taken as spherically symmetric. Explicitly, we assume that the number density in the lens plane is

$$n(R) \propto (R^2 + r_d^2)^{-m/2}. \quad (15)$$

where $m > 1$ determines the asymptotic fall-off of the distribution, and r_d is a central softening parameter. We choose $m = 5/2$ so that the three-dimensional number density, obtained by Abel deprojection of (15), falls off like (distance) $^{-3.5}$, similar to the behaviour observed in the Milky Way (see e.g., Wilkinson & Evans 1999). We choose two different r_d , so that half the satellites are within a (spherical polar) radius $d_{1/2}$ of 100 kpc or 50 kpc respectively of the centre of the main galaxy. The distributions are plotted in Fig. 1. Note that, at least as judged from the case of the Milky Way, we expect half the satellites to lie within 100 kpc, and so $d_{1/2} \sim 100$ kpc is perhaps the more realistic.

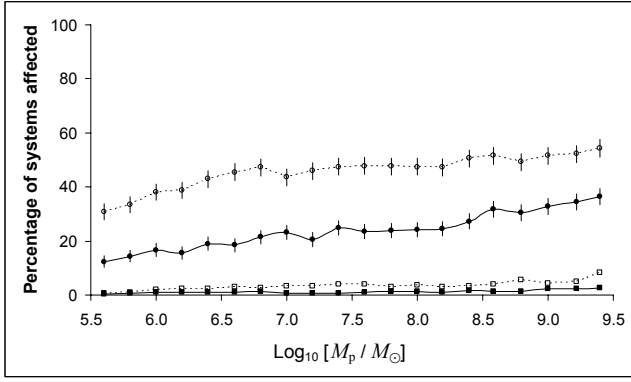


Figure 2. The proportions F_4 of quad (circles) and F_2 of doublet (squares) lens systems that have a flux ratio changed by $\geq 5\%$ by Plummer satellite galaxies, as a function of the mass per satellite galaxy. The total mass in satellites, M_{sat} , is fixed at $5 \times 10^9 M_\odot$ and the scalelength of the distribution at $d_{1/2} = 100$ kpc (solid points and line) and $d_{1/2} = 50$ kpc (open points and dotted line). The lens is a pseudo-isothermal elliptic potential with $\epsilon = 0.1$. Note especially that F_4 is only weakly dependent on how the mass is shared between satellites. The error bars are 2σ of a binomial distribution.

2.2 Numerical Details

For a given source position, the lens equation can be solved numerically by first triangulating the image plane, mapping the grid to the source plane to triangulate the image positions, and then using a multi-dimensional Newton-Raphson procedure.

The satellite galaxies have small effects on the positions of the images and on critical curves and caustics. Their effect is mainly on the ratios between image fluxes. When a satellite galaxy is sufficiently near an image, it changes the magnification of that image. Only if the separation between the satellite and the image is still smaller does image splitting occur. In this paper, we focus on the effect of the satellites on the flux ratios of lenses rather than the image multiplicity. When images split, they are near new critical curves created by the satellite galaxy and are highly magnified, which certainly results in a flux ratio change.

We generate positions of sources randomly to find 1000 five-image and 1000 three-image systems. For each system, the image positions and magnifications are found numerically, both for the main galaxy alone and with satellite galaxies at positions randomly generated according to the distribution (15) (or its 3D deprojection, for the purposes of finding tidal radii). We count the number of systems where the satellite galaxies change the ratio of any two image fluxes by 5% or more (discounting the usually unobservable central images).

3 THE TOTAL MASS IN SATELLITES

3.1 Plummer Satellites

For the moment, let us fix the total mass in satellite galaxies M_{sat} as $5 \times 10^9 M_\odot$ and share it equally among a varying number N of satellites. The lens galaxy is an $\epsilon = 0.1$ pseudo-isothermal elliptical potential, and the satellites are spatially distributed with $d_{1/2} = 100$ kpc. The results are shown in Fig. 2, which illustrates that, over a large range of M_p or N , the proportion F_4 of quads with flux ratios affected by the satellites is only weakly dependent on how mass is apportioned between the satellites. That is, the proportion F_4 is mainly sensitive to the total mass $M_{\text{sat}} = NM_p$

rather than N or M_p . The solid line in Fig. 2 suggests that satellites of mass $10^9 M_\odot$ are only 50% more efficient at altering flux ratios than those of mass $10^7 M_\odot$. The Plummer scale radius r_p , if set differently, can affect the results. For example, fixing r_p to 140 pc for all M_p causes F_i fall off rapidly below $M_p = 10^7 M_\odot$, as the central density of the satellites decreases.

Fig. 2 can be understood qualitatively as follows. The magnification of an image is changed by $\geq 5\%$ – and the flux ratios of the lens system affected – if the image is within a ‘radius of influence’ r_{eff} of a satellite. Here, r_{eff} depends on the location and magnification of the image, as well as the mass of the satellite. (r_{eff} increases with the mass of the satellite and the magnification of the image. Note that there can be an ambiguity in r_{eff} . As a satellite moves closer to the image, the image may be first slightly brightened, before dimming rapidly as the satellite approaches, or first slightly dimmed before brightening rapidly. So, for a large enough satellite, there may be two ranges in which the flux changes by $\geq 5\%$. For the purpose of our rough argument here, however, we ignore this complication.) For a given configuration, the probability that the flux ratio is changed appreciably by satellites depends not only on the number of satellites and their probability distribution in space, but on the individual values of r_{eff} . Even so, ensemble averaging over many image configurations of the same type (e.g. quads) yields an r_{eff} that depends only on the mass of the satellite.

The fractions of quads and doublets that are affected by satellites depend on the fractional area A_{sat} of the lens plane that lies within the circles of influence. That is,

$$\begin{aligned} 1 - F_4 &\approx (1 - A_{\text{sat}})^4 \Rightarrow F_4 \approx 4A_{\text{sat}} - 6A_{\text{sat}}^2, \\ 1 - F_2 &\approx (1 - A_{\text{sat}})^2 \Rightarrow F_2 \approx 2A_{\text{sat}} - A_{\text{sat}}^2, \end{aligned} \quad (16)$$

where r_{eff} , A_{sat} are different for quads and doublets. If A_{sat} is small, the circles of influence do not overlap, so

$$A_{\text{sat}} \propto \sum_{i=1}^N \pi r_{\text{eff}}^{(i)2}. \quad (17)$$

The gently increasing F_i in Fig. 2 over a range of M_p reflects a dependence $r_{\text{eff}}^2 \propto M_p^p$ for $p \gtrsim 1$. For $d_{1/2} = 50$ kpc, the proportional increase in F_4 between, say, $10^7 M_\odot$ and $10^9 M_\odot$ (see dotted line in Fig. 2) is less than for $d_{1/2} = 100$ kpc because of greater overlapping (A_{sat} increases more slowly than $\sum_{i=1}^N \pi r_{\text{eff}}^{(i)2}$). Doublets are much less strongly affected than quads not only because there are only two rather than four images whose fluxes could be affected (hence the $2A_{\text{sat}}$ rather than $4A_{\text{sat}}$ term in (16)), but, more importantly, because their images are typically of much lower magnification.

Let us now allow the total mass M_{sat} in satellite galaxies to vary. Since F_i are not quite independent of how M_{sat} is apportioned between satellites, we need to allow for different individual satellite masses. We draw them from an M^{-2} distribution with cut-offs at $5.0 \times 10^6 M_\odot$ and $5.0 \times 10^9 M_\odot$, and vary N to vary M_{sat} . (Cutoff masses of below 5.0×10^6 were too computationally expensive because many more satellites would have been needed for the same total masses.) The masses of the satellites (along with their positions) are regenerated for each new source position. The results are shown in Fig. 3, where F_i are plotted as a function M_p on a log-log scale. The scalings (16) and (17) can be seen: F_i initially increase \lesssim linearly with M_{sat} (as $A_{\text{sat}} \propto N \propto M_{\text{sat}}$ for a given satellite mass function), until the overlaps between circles of influence can no longer be neglected, after which F_i approach unity asymptotically. The proportions F_i go from 20% to 80% over about one order of magnitude of M_{sat} (this can be seen even more clearly

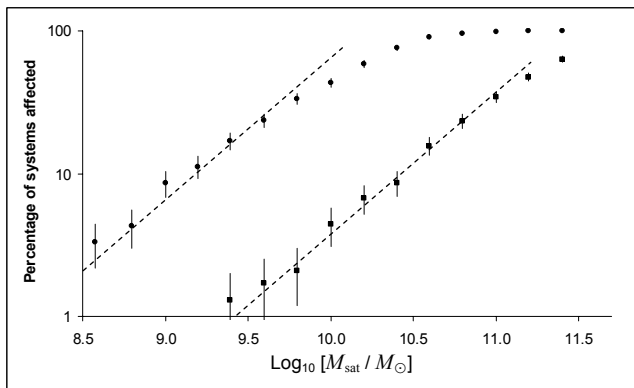


Figure 3. The proportions F_i of quads and doublets (upper and lower curves) as functions of the total mass M_{sat} in Plummer satellites drawn from the M^{-2} distribution, on a log-log scale. Here, $d_{1/2} = 100$ kpc; similar behaviour holds for other $d_{1/2}$ (not illustrated). The dotted lines are of unit gradient: when the percentage of affected systems is low, F_i scales as $\propto M_{\text{sat}}$.

from Fig. 6 in the next section). At all M_{sat} , flux ratios of quads are much more likely to be affected than those of doublets.

3.2 Hernquist Satellites

Since the bound mass M_t of a Hernquist profile satellite depends, through (11) and (14) on its initial mass M and its distance from the main galaxy (generated randomly in this simulation), we cannot repeat §3.1 exactly. We can only fix the total initial mass, apportioning it equally between the varying number of satellites N . More-massive satellites, which are therefore less concentrated, are more prone to tidal disruption: for $d_{1/2} = 100$ kpc, a total initial mass of $1.0 \times 10^{10} M_\odot$ results in a total tidally bound mass of $\sim 7 \times 10^9 M_\odot$ if shared equally between 1000 dwarfs of initial mass $10^7 M_\odot$, and $\sim 6 \times 10^9 M_\odot$ if shared between 10 of initial mass $10^9 M_\odot$. For $d_{1/2} = 50$ kpc these fall to $\sim 6.3 \times 10^9 M_\odot$ and $\sim 5.7 \times 10^9 M_\odot$ respectively. Even more significantly, the most massive satellites cannot stay bound close-in to the main galaxy (whereas smaller satellites *can*), decreasing their chances of lying near the centre of the lens in projection, where the images typically are. This is dramatically illustrated in Fig. 4, where for $d_{1/2} = 100$ kpc the proportion of systems with altered flux ratios only varies weakly with N , whereas for $d_{1/2} = 50$ kpc satellites with $M_t \lesssim 5 \times 10^7 M_\odot$ are much more efficient at changing fluxes than massive ones. However, this result depends on the assumption that a satellite which is highly tidally disrupted ($r_t < r_s$) can be ignored, on the grounds that its mass surface density is so diffuse that it has little effect on the lensing fluxes.

Drawing initial masses from the same M^{-2} distribution as before, and varying N to vary the total bound mass M_{sat} , we obtain Fig. 5, which is the analogue of Fig. 3. The Hernquist profile satellites, which are more extended and diffuse than the Plummer models, are less efficient at altering fluxes.

4 ASTROPHYSICAL APPLICATIONS

4.1 Elliptical Galaxy Lenses

Let us consider several different sets of parameters of elliptical potentials (3) and ask what mass in satellites is required for there to be

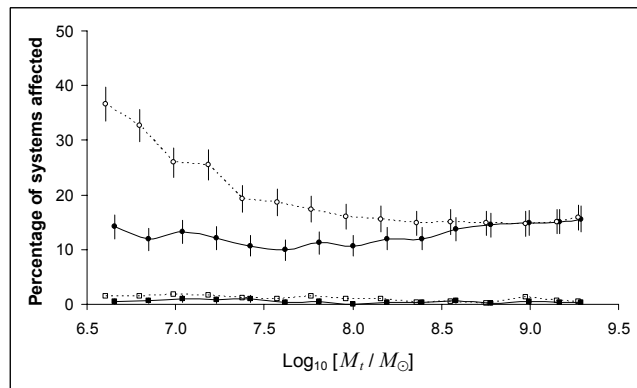


Figure 4. As Fig. 2, but with an initial total mass in Hernquist profile satellites fixed at $1.0 \times 10^{10} M_\odot$. F_i are plotted against the average tidally bound mass per truncated Hernquist satellite.

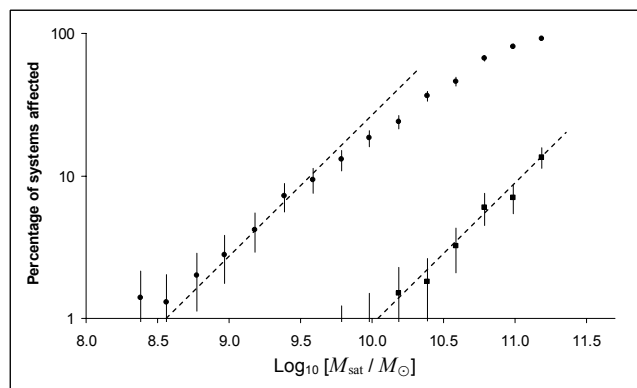


Figure 5. The proportions F_i of quads and doublets (upper and lower curves) as functions of tidal mass M_{sat} in Hernquist dwarfs, $d_{1/2} = 100$ kpc. The dotted lines are of unit gradient.

a significant probability of flux-ratio changes. We first use Plummer model satellites, drawn from the M^{-2} mass function, and again vary the number of satellites to vary the total mass. The results are plotted in Figure 6.

For the moderately elliptic case $\epsilon = 0.1$, masses of $\sim 1.25 \times 10^{10} M_\odot$ are needed for 50% of quadruplets to show anomalous flux ratios if $d_{1/2} = 100$ kpc, decreasing to $\sim 5 \times 10^9$ for $d_{1/2} = 50$ kpc. The lengthscale of the satellite distribution $d_{1/2}$ has a large effect on *both* F_4 and F_2 . As expected, the higher the probability density of satellites in the inner parts of the lens plane (where the images lie), the greater the proportion of anomalous flux ratio systems. Comparing left and right panels, we see that the effect of satellites on flux ratios of quadruplets decreases as ϵ increases – and the quadruplet cross-section increases, while the mean magnification of quads falls. The proportion of doublets F_2 , however, is *not* noticeably affected by the ellipticity ϵ .

Changing the redshifts of lens and source affects these results only through Σ_{cr} , on which E_r in eq (4) and $\kappa_0^{(k)}$ in eq (8) depend. F_i for two sets of redshifts are plotted in Fig. 7, for $d_{1/2} = 50$ kpc and $\epsilon = 0.1$. We see that the results are not very sensitive to different redshifts or different Σ_{cr} . The results are also not very sensitive to the core radius of the pseudo-isothermal elliptic potential, although they *are* affected by its velocity dispersion σ , as shown in Fig. 8. We recall that the velocity dispersion controls the Einstein radius $E_r = \sigma^2 (\xi_0 G \Sigma_{\text{cr}})^{-1}$, with more massive lens galaxies di-

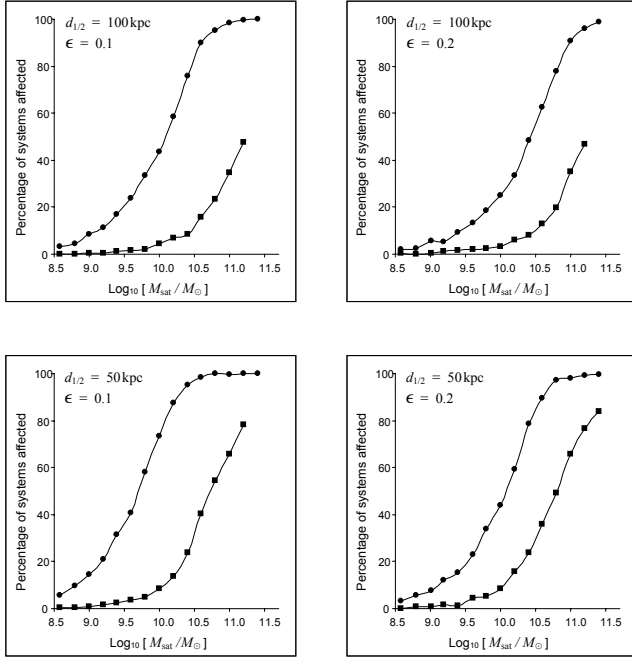


Figure 6. Plots of F_i (circles for quads, squares for doublets) as functions of total mass M_{sat} in Plummer dwarfs, for various parameters. The lens is a pseudo-isothermal elliptic potential with ellipticity ϵ , while the satellite distribution has a characteristic scalelength of $d_{1/2}$ as indicated in the top left of each panel.

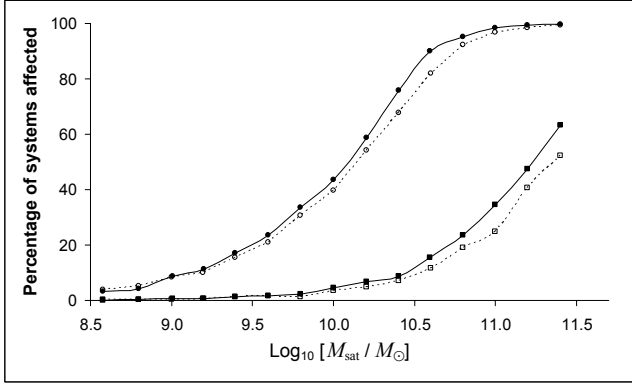


Figure 7. Proportion of systems with flux ratios affected by Plummer model satellite galaxies, as a function of total mass in satellites, for two sets of redshifts. Filled points and solid line: $z_1 = 0.46$, $z_8 = 2.15$ (corresponding to $\Sigma_{\text{cr}} = 2.04 \times 10^9 M_\odot \text{ kpc}^{-2}$). Open points and dotted line: $z_1 = 0.21$, $z_8 = 1.22$ (corresponding to $\Sigma_{\text{cr}} = 3.05 \times 10^9 M_\odot \text{ kpc}^{-2}$). The first set is the median lens- and source-redshifts of known 4-image systems; the second z_1 and z_8 are one standard deviation below the median.

luting the effect of the satellites on flux ratios. A pseudo-isothermal elliptic potential with $\sigma = 300 \text{ km s}^{-1}$ requires ~ 2 times as much mass in satellite galaxies as a $\sigma = 200 \text{ km s}^{-1}$ model for $F_4 = 0.5$, or 50% of the quads to have anomalous flux ratios. However, the Einstein radius of the main galaxy goes as σ^2 , and the projected mass within the Einstein ring as σ^4 , so a given *relative* mass in satellite companions is more likely to affect flux ratios in more massive elliptical lenses.

When the less concentrated, tidally-stripped Hernquist profile satellites are used instead of Plummer models, the effect on flux ratios is significantly weaker: Fig. 9 is the analogue of Fig. 6. The

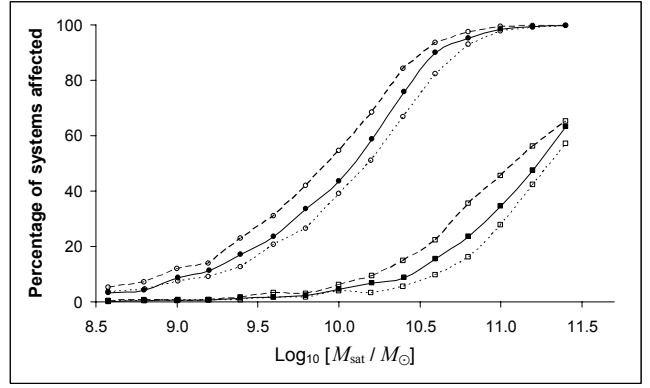


Figure 8. Percentages of systems with flux ratios affected by Plummer model satellite galaxies, as a function of the total mass in satellites, for redshifts $z_1 = 0.46$ and $z_8 = 2.15$, for three different velocity dispersions: $\sigma = 200 \text{ km s}^{-1}$ (dashed line), 250 km s^{-1} (solid line), 300 km s^{-1} (dotted line). The remaining parameters are $\epsilon = 0.1$ and $d_{1/2} = 100 \text{ kpc}$.

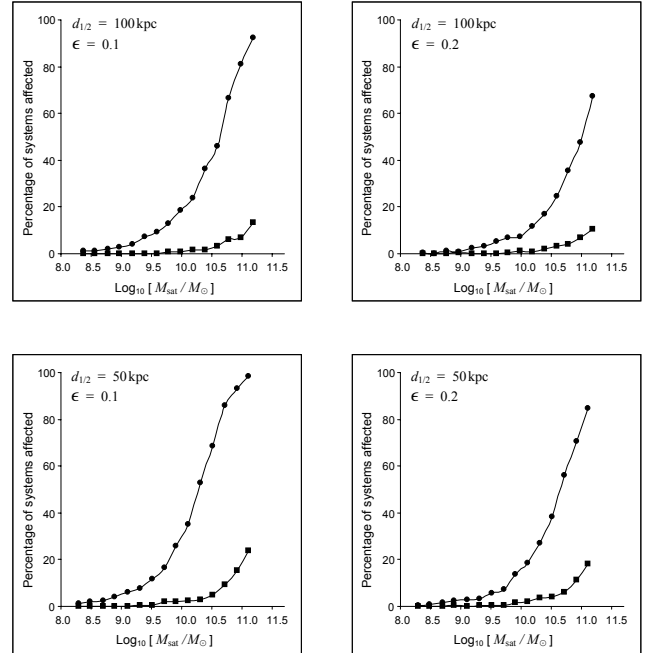


Figure 9. Effect of Hernquist satellites on flux ratios (analogue to Fig. 6).

initial masses of the Hernquist dwarfs are drawn from the same M^{-2} distribution, and F_i are plotted against the total tidal mass in satellites. For the $\epsilon = 0.1$ elliptical potential, if $d_{1/2} = 100 \text{ kpc}$, some $4.5 \times 10^{10} M_\odot$ in satellites is needed for 50% of quadruplet flux ratios to be altered (over three times the mass in Plummer satellites needed), dropping only to 2×10^{10} for $d_{1/2} = 50 \text{ kpc}$ (about eight times the mass in Plummer satellites needed) because of the increased tidal stripping of closer-in satellites.

4.2 Spiral Galaxy Lenses

Now let us change the lens galaxy to an edge-on spiral, using the model based on eqns (5)-(7). Plots of F_i as functions of M_{sat} , for Plummer model satellites, are plotted in Fig. 10 as solid lines alongside those for a pseudo-isothermal elliptic potential as dotted lines. The upper panel shows the model in which the disc is maximal and

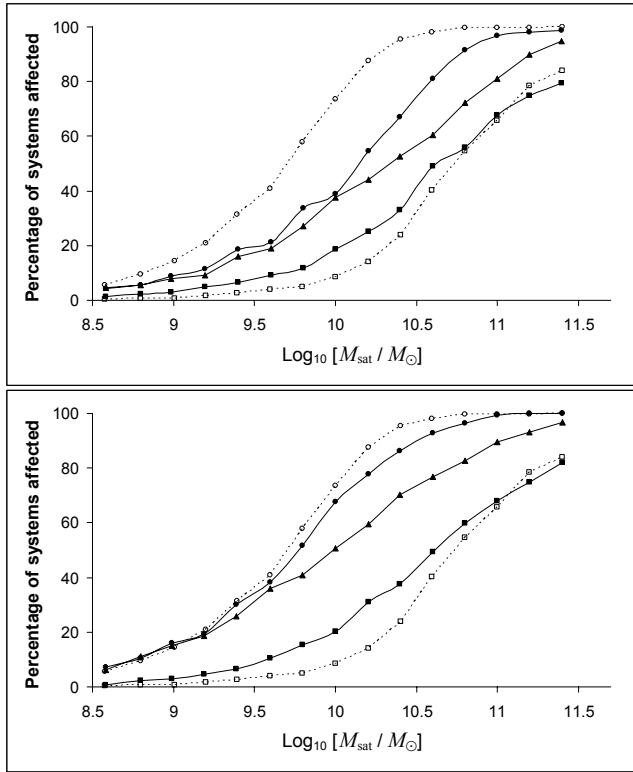


Figure 10. The upper panel shows F_i as functions of the total mass in Plummer satellites, for an edge-on Milky Way with maximal disc (solid lines and filled symbols) and a pseudo-isothermal elliptic potential for comparison (dotted lines and open symbols) with $\sigma = 250 \text{ km s}^{-1}$. The lower panel shows the same quantities but for a sub-maximal disc. Both galaxies are at $z_l = 0.46$, lensing sources at $z_s = 2.15$. $d_{1/2} = 50 \text{ kpc}$. Quads are shown as circles, doublets as squares, and disc triplets as triangles.

provides most of the rotational support in the inner parts, the lower panel shows a model in which the disc is sub-maximal (see Shin & Evans 2007 for a detailed discussion of the lensing properties of these models). There are three solid lines in the panels, as the results are divided according to the five image (in effect, quadruplet), core triplet (in effect, doublet) and disc triplet morphologies.

Compared to a typical elliptical, the flux ratios of maximal disc lens quads are significantly less susceptible to changes through substructure – almost three times the mass in satellite galaxies is needed to affect half the flux ratios. Spiral doublets, however, are slightly more susceptible. This is as expected: the greater the asymmetry of the matter distribution, the larger the 4-image cross-section, the lower the typical magnification of quads and the smaller the effect of satellite galaxies on the 4-image flux ratios. (So disc triplets, with typical magnifications in between quads and doublets, are also in between in susceptibility to flux changes.) Indeed, we do not expect many anomalous flux ratios in disc galaxy lenses to be caused by the satellite galaxies in their haloes unless these satellites total at least $\gtrsim 10^{10} M_\odot$ in mass, that is, $\approx 10\%$ of the luminous galaxy mass! (And *that* assumes the satellites are distributed with $d_{1/2} = 50 \text{ kpc}$.) On moving to the sub-maximal case, the 4-image and disc triplet cross sections are substantially reduced, and so the numbers return towards their values in the elliptical galaxy case.

Note that we have compared the effects of a typical spiral with asymptotic circular speed of $v_0 \approx 220 \text{ km s}^{-1}$ to a typical elliptical with line-of-sight velocity dispersion of $\sigma = 250 \text{ km s}^{-1}$.

This makes sense, as early-type galaxies are more massive than late-type. If instead we were to carry out the comparison using $\sigma = v_0/\sqrt{2}$, so that the kinematic properties of the models were comparable, then the elliptical would have a lower velocity dispersion and so the discrepancy between the effects of spirals and ellipticals would be increased (see Figure 8).

4.3 Visible Substructure

Some flux anomalies appear to be attributable to single dwarf galaxies. The most obvious examples are the Sixth Object in MG0414+0534 (Schechter & Moore 1993) and G2 in CLASS B2045+265 (McKean et al. 2007). In both these cases, a single piece of substructure gives a substantial improvement in the fit of a smooth model of the lens galaxy. An interesting question is – if flux ratio anomalies are due to substructure – how often might we expect to see a visible counterpart? At the typical redshifts of the lenses, only the very largest dwarf galaxies can be detected with ground-based telescopes, of course.

This question can be answered by simulations in which the satellites are divided into two populations – N_1 dark satellites of low mass M_1 and N_2 bright satellites of high mass $M_2 \gg M_1$ – and flux-ratio changes are sought for the two populations separately and together. Some sample results of the simulations are shown in Table 1 for the usual $\epsilon = 0.1$ pseudo-isothermal elliptic potential with $d_{1/2} = 100 \text{ kpc}$. Note that, for the Plummer satellites, when the ratio of the total mass in population 1 to total mass in population 2 is 1:1, then the number of systems with anomalous flux ratios caused by population 1 as compared to population 2 is roughly in the ratio of 2:3, and a 3:2 mass ratio gives a roughly 1:1 effect. For the Hernquist satellites, a 1:1 mass ratio gives 1:1 effect. This confirms the observations of §3 that a $10^9 M_\odot$ Plummer-model dwarf spheroidal is only $\sim 50\%$ more efficient at perturbing fluxes than a $10^7 M_\odot$ one, and more-massive Hernquist dwarfs are *no* more efficient than less massive ones. So from Table 1, we see that the most massive satellites do not contribute very disproportionately to anomalous flux ratios.

The neat correspondence between ratios is not seen for 10:1 mass ratios because F_4 increases sub-linearly with mass: e.g. a single $10^9 M_\odot$ in Plummer satellite changes fluxes in 12% of quads, but four of them change fluxes in 28%, not 48%, of quads. However, it is confirmed that $\sim 85\%$ of systems with affected fluxes still have affected fluxes if the 10% of mass in massive satellites is removed.

The fraction of observed anomalous flux ratio systems with visible (and therefore high mass) culprits is actually quite high. Of the six four-image lens systems proposed by Dalal & Kochanek (2002), three (B2045+265, MG0414+0534, B1608+656) have identified, visible substructure that may cause the flux perturbation. If this datum is taken at face value, it suggests that about half the mass in substructure is in dwarf galaxies large enough to be optically identified. Simulations, however, tend to find that the satellite masses behave more like an M^{-2} distribution. This implies that there is equal mass in equal decades, and therefore that each decade is responsible for the causing roughly the same number of flux ratio anomalies (the $10^9 M_\odot$ decade causing only 50% more than the $10^7 M_\odot$ decade).

One resolution of this difficulty is to postulate that the visible dwarf has been mistakenly designated as the culprit and that the anomalous flux ratio is really produced by another dark satellite. A hint that this may sometimes be the case is given by the unrealistically large flattening deduced for satellite G2 in CLASS

Table 1. The proportion F_4 of quads with anomalous flux ratios for five runs of the two-population model. Here, the satellite populations have $d_{1/2} = 100$ kpc and the elliptical lensing galaxy has the standard parameters. Population 1 satellites have mass $1.0 \times 10^7 M_\odot$, while population 2 satellites have mass $1.0 \times 10^9 M_\odot$. (For Hernquist satellites, these are *initial* masses.) The Plummer model Population 2 contributes to F_4 by $\sim 50\%$ more than population 1 satellites, whilst the two Hernquist-model populations contribute equally.

Satellite Profile	$N_1 M_1$ (M_\odot)	$N_2 M_2$ (M_\odot)	F_4 (Both pops)	$F_{4,1}$ (Pop 1 only)	$F_{4,2}$ (Pop 2 only)	$N_1 M_1 : N_2 M_2$	$F_{4,1} : F_{4,2}$
Plummer	1.0×10^{10}	1.0×10^9	43.2%	37.3%	12.2%	10 : 1	3.1 : 1
Plummer	5.0×10^9	5.0×10^9	45.6%	21.5%	34.5%	1 : 1	1 : 1.6
Plummer	6.0×10^9	4.0×10^9	44.3%	23.4%	28.1%	3 : 2	1 : 1.2
Hernquist	2.0×10^{10}	2.0×10^9	28.4%	25.1%	5.1%	10 : 1	4.9 : 1
Hernquist	1.2×10^{10}	8.0×10^9	22.8%	16.3%	10.6%	3 : 2	3.1 : 2
Hernquist	1.0×10^{10}	1.0×10^{10}	20.9%	13.2%	12.1%	1 : 1	1.1 : 1

B2045+265 using model-fitting in McKean et al. (2007). In other words, it may simply be a chance effect that many anomalous flux ratio systems appear to have visible objects at or near the Einstein radius. The probability that a large dwarf lies close to the Einstein radius is easily computed from eq (15). When $d_{1/2} = 100$ kpc, then there is a 10% probability of a large dwarf lying within two Einstein radii and 3% within one. This still does not seem large enough to explain the effect, but caution is needed as there may be other supplies of substructure along the line of sight for some of the lenses in groups and clusters, like B1359+154. It is worth noting that simulations (see e.g. Zentner et al. 2005) can sometimes yield highly anisotropic distribution of substructure in simulated halos: the projected subhalo mass within 10 kpc can vary by factor of 10 depending on viewing angle. In this case, sightlines which project massive satellites onto small radius are also much more likely to project other satellites onto small radius. This may mean that our computed probabilities of 3-10 % may be on the low side.

Another possible resolution of the difficulty is that luminous satellites, the baryons in which have cooled and condensed, may be much more centrally concentrated than dark satellites. In other words, it is possible that luminous satellites would have a much larger effect on flux ratios than their dark brethren because they are structurally different and more compact. Of course, the effect of baryons on dark haloes is subject to considerable uncertainties. This effect must be small for dwarfs like Draco, with a mass-to-light ratio of > 350 (Kleyna et al. 2001), although it may be more significant for satellites like the Large Magellanic Cloud with a mass-to-light ratio of ~ 5 (Alves 2004). It is also known that semi-analytic calculations of galaxy formation lead to too many compact, luminous satellites, as compared to what is seen around the Milky Way (see e.g., Koposov et al. 2007). The bright satellites predicted by semi-analytic theories are much too concentrated, suggesting that this effect is overplayed in the modelling.

Nonetheless, the effect certainly exists at some level and is worth investigating. Baryon condensation may increase the central density by a factor of between 4 and 160 (Gnedin & Zhao 2002), although the larger numbers are probably more appropriate for galaxies like the Milky Way rather than satellite galaxies. We change the lengthscale r_s of the Hernquist model to mimic the result of baryon condensation and quantify the extra effect, compared to dark Hernquist satellites, that highly-concentrated luminous satellites could have on flux ratios. (The Plummer satellites are already so compact that changing the Plummer scale radius makes no appreciable difference even when the central density is raised by a factor 100.) The Hernquist density law (13) means that the central density goes as r_s^{-2} , so we modify the scalelength-to-mass relation (14) to

Table 2. The (average) tidal mass M_{sat} in Hernquist satellites of untruncated mass $10^9 M_\odot$ needed to affect fluxes in 50% of four-image systems, for various q . The elliptical galaxy has the standard parameters and the scalelength of the spatial distribution of satellites is $d_{1/2} = 100$ kpc.

Satellite Profile	N	M_{sat} (M_\odot)
Hernquist (dark)	100	5.6×10^{10}
Hernquist ($10\times$ concentration)	20	1.5×10^{10}
Hernquist ($100\times$ concentration)	12	1.1×10^{10}

$$r_s = q 10^{-4} \sqrt{M_t/M_\odot}, \quad (18)$$

where $q = 1, 1/\sqrt{10}$, or 0.1, corresponding to central densities of 1, 10 and 100 times that of the dark (uncontracted) Hernquist profile. The number of satellites of initial mass $10^9 M_\odot$ needed to affect flux ratios in 50% of four-image systems (all other parameters being the same as in Table 1) is shown in Table 2. Almost four times the tidal mass in massive dark satellites is required, compared to massive luminous satellites with 10 times the central density, to affect the same proportion of flux ratios. Raising the central density a further factor of 10 has a smaller effect. The increasing effect on fluxes seen with decreasing r_s is amplified by the extra resistance to tidal disruption of the more-concentrated satellites.

Table 3 shows the results of two-population models, in which population 1 are dark satellites of initial mass $10^7 M_\odot$ and population 2 are bright satellites of initial mass $10^9 M_\odot$, with 10 or 100 times the central density of their dark brethren. The fraction of anomalous flux ratio systems caused by bright substructure is now impressively high – for example, the second line of the table tells us that 42 % of systems have anomalous flux ratios, of which 28 % remain anomalous when the dark population is removed. In other words, over half of the anomalous flux ratio systems are caused, at least in part, by bright satellites. This is close to the statistics on observed systems – although caution is needed as large compression factors like 10 or 100 may well cause the importance of this effect to be overestimated for satellite galaxies.

5 CONCLUSIONS

It remains unclear whether dark matter satellites and substructure are responsible for anomalous flux ratios in strong lensing. Dalal & Kochanek (2002) originally studied a sample of 7 radio-loud four-image lens systems and claimed evidence of anomalies in 6

Table 3. The proportion F_4 of quads with anomalous flux ratios for three runs of the two population model, with the same parameters as in Table 1 but where population 2 satellites have increased central density. As the compression increases (q decreases), the tidally bound mass of population 2 satellites increases, but their effect on fluxes increases disproportionately, outstripping the effect of the diffuse low-mass population 1 satellites. The difference caused by a factor 10 increase in central density is much larger than the difference caused by an extra step to a 100-fold increase.

Satellite Profile	N_1 (M_\odot)	N_2 (M_\odot)	$M_{\text{sat}}^{\text{pop1}}$ (M_\odot)	$M_{\text{sat}}^{\text{pop2}}$ (M_\odot)	F_4 (Both pops)	$F_{4,1}$ (Pop 1 only)	$F_{4,2}$ (Pop 2 only)
Hernquist	1200	8	7.4×10^9	4.5×10^9	23%	16%	11%
Hernquist (Pop 2 with $10\times$ concentration)	1200	8	7.4×10^9	6.0×10^9	42%	16%	28%
Hernquist (Pop 2 with $100\times$ concentration)	1200	8	7.4×10^9	7.2×10^9	48%	16%	36%

of them. This seemingly suggests that anomalous flux ratios are very common. Here, we have carried out a theoretical study of the frequency of flux ratio anomalies as a function of lensing galaxy and dark matter substructure parameters.

The likelihood that satellites affect flux ratios in strong lenses depends on their mass profile. Here, we considered compact Plummer spheres and diffuse, tidally stripped Hernquist profiles for our satellites, with the satellite size scaling as a power of mass. As the Hernquist satellites are more extended than the Plummer models, they therefore have a smaller effect on image fluxes – typically about 3 times the mass is needed to generate the same numbers of anomalous flux ratios.

The probability that strong lensing flux ratios are affected by satellites is crucially dependent on their spatial distribution. The characteristic lengthscale $d_{1/2}$ has a large effect on the fraction of lenses with affected flux ratios. Our spatial distributions of satellite galaxies are inspired by the observational data on the Milky Way, for which the satellite number density falls off as $\hat{r}^{-3.5}$ in three-dimensions with a lengthscale of $d_{1/2} \sim 100$ kpc. For such distributions, most satellites are too far out to affect the fluxes of images. For example, even with Plummer satellites, a mass of $\sim 3 \times 10^9 M_\odot$ is needed for 20 % of quadruplets to show anomalous flux ratios for a typical elliptical galaxy, rising to $\sim 1.25 \times 10^{10} M_\odot$ for 50 %. Lenses that are edge-on spiral galaxies with maximum discs (like the Milky Way) are more resistant to flux changes by satellites, so the mass in satellites and substructure has to be roughly a factor of 3 times as great for the same proportion of quads to be affected. To obtain anything like the apparent abundance of anomalous flux ratios, then the scalelength of the substructure has to be different to what is known for the Milky Way satellites.

Whether the flux ratios in a lens system are affected by satellites is sensitive to the total mass in satellites, but more weakly dependent of how this mass is apportioned between them. For Plummer model satellites, the probability that a given satellite changes a flux ratio increases with its mass only slightly faster than linearly, at least when its mass is between $\sim 5 \times 10^6 M_\odot$ and $\sim 10^9 M_\odot$. For example, satellites of mass $\sim 10^9 M_\odot$ are only responsible for the causing $\sim 50\%$ more flux ratio anomalies than those of mass $\sim 10^7 M_\odot$. For Hernquist model satellites, more massive ones seem no more efficient (per unit mass) at changing fluxes; indeed, more massive dwarfs, being more prone to tidal disruption, might even be *less* efficient than lighter, more compact ones. One interesting consequence is that, if matter in dark satellites is not predominantly in the most massive ones, then the contribution of the most massive satellite galaxies to flux ratio anomalies should not be predominant.

In the light of this, the fact that so many anomalous flux ratios systems have optically identified substructure seems at outset surprising. There seem to be two possible explanations. First,

the visible substructure may have been wrongly identified as the cause, whereas dark substructure may be the true culprit. A large dwarf galaxy may by chance be projected close to the Einstein radius, whereas unrelated dark substructure may be the major cause of the anomaly. Second, visible satellites may be more concentrated than their dark cousins, a physical effect that may naturally arise from baryon condensation. Compression factors causing an enhancement of the central density by a factor of 10 in bright satellites seem to be ample to give a satisfactory explanation of the observed statistics. Nonetheless, such high compression factors are probably implausible except for the largest satellite galaxies. This seems to be in accord with the results of Macciò et al. (2006), who found that including baryons in numerical simulations did not help in reconciling simulation results with the statistics of anomalous flux ratios.

Finally, we remark that the likelihood that flux ratios are affected depends on the ellipticity of the main lens galaxy, but this dependence is much stronger in quads than doublets. This is a consequence of high magnification images being more easily affected by a dwarf galaxy than low magnification ones. Quads are more highly magnified than doublets (the disc triplets of spirals are in between), and changing the ellipticity of the main galaxy changes the typical magnification of quads more than it changes that of doublets. Generally, the greater the ellipticity the less the effect of satellite galaxies. For example, a given mass M_{sat} of dwarf satellites around a typical edge-on maximum-disc spiral galaxy is significantly less likely to change image flux ratios than M_{sat} around a typical elliptical galaxy, even though the spiral is less massive than the elliptical.

ACKNOWLEDGEMENTS

We thank the referee for some helpful comments. EMS thanks the Commonwealth Scholarship Commission and the Cambridge Commonwealth Trust for the award of a Studentship. NWE thanks Neal Jackson for some insightful discussions. This work has been supported by the ANGLES network.

REFERENCES

- Alves D.R., 2004, ApJ, 601, L151
- Belokurov V. et al., 2006, ApJ, 647, L111
- Belokurov V. et al., 2007, ApJ, 654, 897
- Bradač M., Schneider P., Lombardi M., Steinmetz M., Koopmans L.V.E., Navarro J.F., 2004, A&A, 423, 797
- Dalal N., Kochanek C.S. 2002, ApJ, 572, 25
- Dinescu D.I., van Altena W.F., Girard T.M., López C.E., 1999, AJ, 117, 1792

Diemand J., Kuhlen M., Madau P. 2007, ApJ, in press,
 arXiv:astro-ph/0703337
 Efstathiou G. 1992, MNRAS, 256, 43P
 Evans N.W., Hunter C. 2002, ApJ, 575, 68
 Evans N.W., Witt H.J., 2003, MNRAS, 345, 1351
 Fassnacht, C.D., Womble, D.S., Neugebauer, G., Browne, I.W.A.,
 Readhead, A.C.S., Matthews, K., & Pearson, T.J. 1996, ApJ,
 460, L103
 Fassnacht C.D., et al., 1999, AJ, 117, 658
 Fellhauer M., et al., 2006, ApJ, 651, 167
 Gnedin O.Y., Zhao H., 2002 MNRAS, 333, 299
 Hernquist L., 1990, ApJ, 356, 359
 Hunter C., Evans N.W., 2001, ApJ, 554, 1227
 Johnston K.V., Spergel D.N., Hernquist L., 1995, ApJ, 451, 598
 Kassiola A., Kovner I., 1993, ApJ, 417, 450
 Kleyna J.T., Wilkinson M.I., Evans N.W., Gilmore G.F., 2001,
 ApJ, 563, L115
 Klypin, A., Kravtsov, A.V., Valenzuela, O., & Prada, F. 1999, ApJ,
 522, 82
 Kochanek C.S., Dalal N. 2004, ApJ, 610, 69
 Koposov S., et al. 2007, ApJ, submitted, (arXiv:0706.2687)
 Kravtsov, A.V., Gnedin, O.Y., & Klypin, A.A. 2004, ApJ, 609,
 482
 Macciò, A.V., Miranda M. 2006, MNRAS, 368, 599
 Macciò, A. V., Moore, B., Stadel, J., & Diemand, J. 2006, MN-
 RAS, 366, 1529
 Mao S., Schneider P., 1998, MNRAS, 295, 587
 Mao S., Jing Y., Ostriker J.P., Weller J. 2004, ApJ, 604, L5
 McConnachie A.W., Irwin M.J., 2006 MNRAS 365, 1263
 McKean J.P., Koopmans L.V.E., Flack C.E., Fassnacht C.D.,
 Thompson D., Mathews K., Blandford R., Readhead A.C.S.,
 Soifer B., 2007, MNRAS, 378, 109
 Metcalf R.B., Madau P., 2001, ApJ, 563, 9
 Miyamoto M., Nagai R., 1975, PASJ, 27, 533
 Möller O., Blain A.W., 1998, MNRAS, 299, 845
 Moore, B., Ghigna, S., Governato, F., Lake, G., Quinn, T., Stadel,
 J., & Tozzi, P. 1999, ApJ, 524, L19
 Moore B., Diemand J., Madau P., Zemp M., Stadel J. 2006, MN-
 RAS, 368, 563
 Navarro, J.F., Frenk, C.S., White, S.D.M. 1996, ApJ, 462, 563
 Rusin, D., et al. 2001, ApJ, 557, 594
 Schechter P.L., Moore C.B. 1993, AJ, 105, 1
 Schneider P., Ehlers J., Falco E.E., 1992, Gravitational Lenses,
 Springer-Verlag, New York
 Shin E.M., Evans N.W., 2007, MNRAS, 374, 142
 Wilkinson, M.I., & Evans, N.W., 1999, MNRAS, 310, 645
 Wilkinson M.I., Klenya J, Evans N.W., Gilmore G., 2002, MN-
 RAS 330, 778
 Willman B., et al., 2005, ApJ 626, L85
 Zentner, A.R., Kravtsov, A.V., Gnedin, O.Y., & Klypin, A.A.,
 2005, ApJ 629, 219
 Zucker, D.B., et al., 2006a, ApJ, 643, L103
 Zucker, D.B., et al., 2006b, ApJ, 650, L41